nature communications

Article

https://doi.org/10.1038/s41467-024-55472-8

Elastic, strong and tough ionically conductive elastomers

Received: 11 August 2024

Accepted: 13 December 2024

Published online: 06 January 2025

Check for updates

Burebi Yiming[1,2], Simon Hubert[3], Alex Cartier[1], Bruno Bresson[1], Gabriel Mello[1], Armelle Ringuede[3] & Costantino Creton[1]

Stretchable elastic materials with high strength, toughness, and good ionic conductivity are highly desirable for wearable devices and stretchable batteries. Unfortunately, limited success has been reported to attain all of these properties simultaneously. Here, we report a family of ionically conductive elastomers (ICEs) without compromise between mechanical properties (high stiffness, reversible elasticity, fracture resistance) and ionic conductivity, by introducing a multiple network elastomer (MNE) architecture into a low T_g polymer. The ICEs with the MNE architecture exhibit a room temperature ionic conductivity of the order of 10^{-6} S.cm^{-1} and stress at break of ~8 MPa, whereas the simple networks without an MNE architecture show two orders magnitude lower ionic conductivity (10^{-8} S.cm^{-1}) and comparably low strength (<1.5 MPa) at 25 °C than their MNE architecture based counterparts. The MNE architecture with a low T_g monomer combines the stiffness and fracture toughness given by sacrificial bond breakage while improving ionic conductivity through increased segmental mobility.

Stretchable ionically conductive materials have been instrumental in the development of soft ionotronic devices, i.e. relying on soft conductive materials whose functions are governed by the motion of ions, and batteries[1–4]. The ultimate goal being to design deformable environmentally friendly soft devices with long-term stability and durability. To meet these stringent requirements, ionic conductors not only should have a high ionic conductivity, but should also resist many cycles of high-strain deformation. Although the required deformability does not need to be that high (comparable to skin i.e., 30–50%), the materials need to have sufficient mechanical performance (i.e., stiffness, strength, and toughness) to avoid device failure due to external damage, combined with elastic recovery and good fatigue resistance to function under a large number of cyclic stretches.

Liquid-based stretchable ionically conductive materials (i.e., hydrogels, organogels, and ionogels) can be obtained by dissolving salts (i.e., NaCl, LiCl) or ionic liquids (i.e., ILs for short) into stretchable polymer networks. Such materials are conductive when powered by an external electrical field due to the presence of mobile ions. Salt-containing hydrogels were first considered as a candidate for soft ionotronic devices designed by the layer-by-layer arrangement of hydrogel-elastomer sheets[2] and to design stretchable batteries[5,6], either as the stretchable electrode[5] or as the stretchable substrate[6].

However, these highly conductive hydrogels and organogels are not stable over time due to evaporation or leakage of solvents (i.e., water or organic solvents)[1–3]. Ionogels, consisting of polymer networks and ILs, inherit the excellent electrical properties of ILs (i.e., ionic conductivity, wide electrochemical window), non-volatility (negligible vapor pressure), and thermal stability, and those of polymer networks (i.e., mechanical properties, deformability, solid-like behavior)[7], making them more stable compared to hydrogels and organogels. Reported ionogels are, however, rather soft (Young's modulus <0.1 MPa) and weak (fracture strength <1 MPa)[8–13], limiting their applications mostly within the scope of sensors[8,9,13], in which there are no strict requirements for strength.

More recently, strong and tough ionogels have been reported using phase separation strategies[14], supramolecular networks[15], or

[1]Laboratoire Sciences et Ingénierie de la Matiére Molle, ESPCI Paris, CNRS, PSL University, Paris, France. [2]Key Laboratory of Soft Machines and Smart Devices of Zhejiang Province, Center for X-Mechanics, Department of Engineering Mechanics, Zhejiang University, Hangzhou, China. [3]Chimie Paris Tech, CNRS, Institut de Recherche de Chimie Paris, PSL University, Paris, France. e-mail: costantino.creton@espci.psl.eu

double network polymer architecture[10,16]. Yet, these ionogels show a large hysteresis loop under cyclic loads and a slow recovery of the mechanical properties, making them problematic under cyclic deformations. Highly stretchable barely crosslinked ionogels have also been reported based on nanocomposites[17] but they do not have a high strength[8,9,18] and suffer from creep. In these ionogels, ILs act as plasticizers leading to a tradeoff between ionic conductivity and mechanical performance[8–10,19]. This observed tradeoff between ionic conductivity and mechanical properties stems from general principles. Making a soft material tough requires introducing energy dissipation mechanisms to prevent crack nucleation and growth[20]. The easiest way to do that is by making the material viscoelastic or viscoplastic. Theory predicts[21] and experiment confirms[22] that viscoelastic or viscoplastic materials are tough. However, pronounced viscoelasticity and rate-dependent dissipative mechanisms reduce segmental mobility by increasing internal friction, potentially affecting properties, such as ionic conductivity[23,24]. Furthermore, rate-dependent dissipative mechanisms impart toughness in a single stretch to failure, but do not impart fatigue resistance as recently pointed out[25,26]. To increase one property, one has to sacrifice the other[8–10,19,27].

This trade-off is even more important for liquid-free stretchable ionic conductors or ionically conducting elastomers (ICE). Conductivity is boosted in this case by adding lithium salts (i.e., LiTFSI, $LiClO_4$) to stretchable polymer networks that can solvate them[28–33], or by utilizing intrinsically conductive polymers such as polymerized ionic liquids (i.e., PILs)[34,35], or polymerizable deep eutectic solvents (i.e., PDESs)[36–39]. These ionic conductors do not contain any leakable components and some have been reported with a comparable ionic conductivity as that of some gel-based ionic conductors[33,34]. Yet the reported liquid-free ionically conducting elastomers with high ionic conductivity show excellent mechanical properties because of viscoelastic energy dissipation[40–43] which makes them susceptible to fatigue damage under cyclic loading and leads to a significant drop in stretch at break at high temperatures, limiting their applications near room temperature. For this reason, reversible elasticity, a classic property of engineering elastomers, combined with toughness and high ionic conductivity remains a challenge.

An effective strategy to achieve highly elastic elastomers with remarkable stiffness, strength, and toughness is to embed a highly pre-stretched network into a lightly cross-linked network, so-called multiple network elastomers (MNE)[44]. Sacrificial covalent bonds in these highly pre-stretched first networks act as energy dissipators at high strain only, thereby endowing these elastomers with reversible elasticity up to at least 50% strain but also high toughness and strength by strain hardening at high strains[26]. The maximum extensibility of the strands of the filler network and the fraction of the extensibility created by the swelling steps are the two parameters that determine the elastic properties of the multiple network elastomers, nearly independent of the temperature or of the monomers used to make the network[45,46].

Inspired by this work, we hypothesized that this network design strategy could be transposed to highly elastic yet tough ICEs. In this work, we prepare covalently crosslinked networks made from binary mixtures of monomers ethylene glycol methyl ether acrylate (MEA) and isobornyl acrylate (IBA) (Fig. 1a) containing lithium salt, referred to as P(MEA-*co*-IBA) filler networks, with a T_g of −8 °C. These filler networks are isotropically pre-stretched by swelling them in an MEA monomer solution containing lithium salt (the homopolymer of which

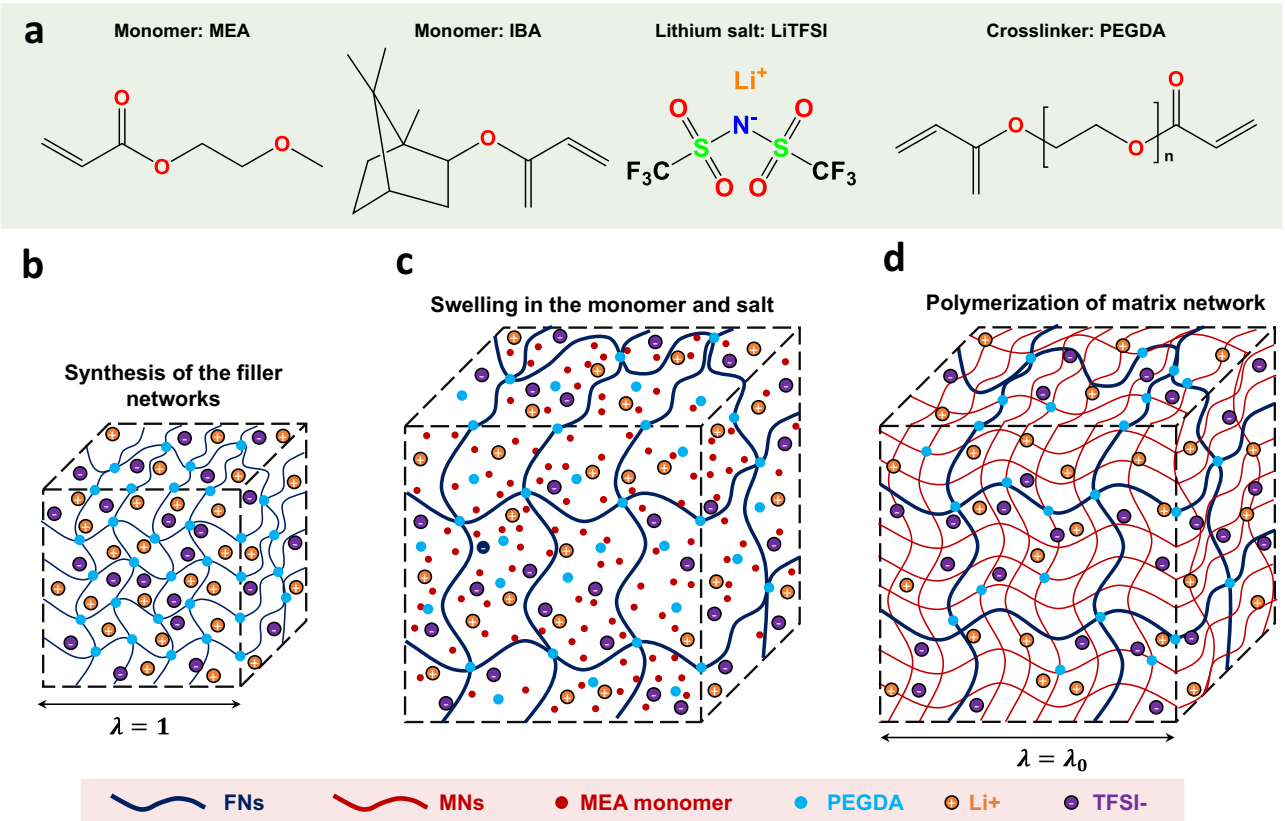

Fig. 1 | Synthesis of ICEs with distinct levels of pre-stretch λ_0. a Molecular structure of monomers of MEA and IBA, lithium salt LiTFSI, and crosslinker PEGDA, respectively. **b** Synthesis of the FNs containing a certain amount of LiTFSI. **c** Swelling of the FN ICEs in the precursor solution of the second network, containing MEA, LiTFSI, PEGDA and HMP. **d** Polymerization of matrix networks. The dark blue lines represent the copolymer/homopolymer networks of P(MEA-co-IBA)/P(MEA), whereas the red lines indicate the second network polymer chains; red and light blue dots indicate MEA and PEGDA, respectively; cations (Li^+) and anions ($TFSI^-$) in the LiTFSI were given by orange and purple circles.

Table 1 | Mechanical and electrical properties of the P(MEA-co-IBA)(λ_0)-ICE(1) series with different pre-stretched networks

Sample name	λ_0	λ_b	*E* (MPa)	*s* (MPa)	$\Gamma_c\left(\mathrm{kJm^{-2}}\right)$	$\sigma(\mathrm{S.cm^{-1}})$
P(MEA-co-IBA) (1)-ICE(1)	1	6.4 ± 0.2	0.37 ± 0.015	1.34 ± 0.05	2.8 ± 0.2	4.5×10^{-8}
P(MEA-co-IBA) (1.54)-ICE(1)	1.54	4.4 ± 0.1	0.43 ± 0.01	5.4 ± 0.17	3.2 ± 0.5	2.43×10^{-6}
P(MEA-co-IBA) (2.36)-ICE(1)	2.36	4.5 ± 0.3	0.5 ± 0.03	6.7 ± 0.2	4.5 ± 0.3	2.05×10^{-6}

has a T_g of −34 °C). Following a second or a third swelling and polymerization step, we obtain ionically conducting elastomers with an MNE architecture and we characterize both their mechanical properties in large strain and their ionic conductivity at different temperatures. We further show that this strategy can be extended to P(MEA).

Results and discussion

To synthesize the ICEs with pre-stretched networks, we combine the method of Chen et al.[47] to make MNE and Yiming et al.[41] method to impart the materials with ionic conductivity. As shown in Fig. 1a, ethylene glycol methyl ether acrylate (MEA) and isobornyl acrylate (IBA) are used as monomers, lithium bis (trifluoromethane sulfonimide) (LiTFSI), poly (ethylene glycol diacrylate) (PEGDA), 2-hydroxy-2-methylpropiophenone (HMP) are used as electrolyte salt, crosslinker, and UV initiator. Synthesis of the multiple network ICEs occurs in several steps. First, a densely crosslinked network is synthesized using either a copolymer of Poly-(MEA-*co*-IBA) or a homopolymer of Poly-(MEA) via free-radical UV polymerization (Fig. 1b) in the presence of LiTFSI. The samples synthesized in this step are referred to as filler networks (i.e., FNs for short). Then these well-crosslinked ICEs are immersed in a precursor solution composed of monomer MEA, LiTFSI, crosslinker, and UV initiator (details are given in the methods section), and are swollen to equilibrium in the glovebox filled with nitrogen at ~ −13–15 °C (Fig. 1c). After UV irradiation, we obtain transparent ICEs containing a pre-stretched FN (Fig. 1d). By changing the concentration of LiTFSI or monomer composition in the FNs, a series of ICEs with distinct mechanical and electrical properties can be synthesized. Figures S2–S3 suggest that the samples are sensitive to ambient water due to the presence of lithium ions. Therefore, all the samples were stored in the glove box to avoid moisture-absorption-induced property changes before any characterization test was performed.

The synthesized ICEs are named either P(MEA-*co*-IBA)(λ_0)-ICE(*x*) or P(MEA)(λ_0)-ICE(*x*), where the P(MEA-*co*-IBA)/P(MEA) represents the networks used in the FNs; the copolymer P(MEA-*co*-IBA) is synthesized based on the binary mixture of monomers of MEA and IBA, whereas the homopolymer P(MEA) is synthesized utilizing only the monomer of MEA; the ICE is the abbreviation of ionically conductive elastomer, λ_0 is the pre-stretch of the filler networks determined by the swelling equilibrium, and *x* represents the molar concentration of LiTFSI in the FNs. A summary of the nomenclature and chemical composition of the samples is shown in Table S1. It is clear from the table that the fraction of IBA (if used) decreases with increasing swelling/polymerization steps since only MEA was used as a monomer in the swelling steps. The fraction of LiTFSI decreases or is nearly constant depending on the amount added into the networks from the swelling solution in each step. The degree of pre-stretch (λ_0) is calculated from the volume fraction (ϕ_{FN}) by using the following Eq. (1)[45]:

$$\lambda_0^3 = \frac{1}{\phi_{FN}} \tag{1}$$

The uniaxial extension tests were performed with dumbbell-shaped samples to assess their stiffness (Young's modulus, *E*), stress at break (strength, *s*), and stretch at break (λ_b) (Fig. S4). Note that the stretch at break λ_b and the degree of pre-stretch λ_0 mentioned in this work are two very different parameters. λ_b is obtained from stress-stretch curves in uniaxial tension whereas λ_0 is obtained from the volume fraction of the stiff filler network in the material, as discussed in a recent publication[46]. Fracture experiments were carried out on single-edge notch samples[48,49] to extract the fracture energy (Γ_c) using the Greensmith Approximation (Fig. S5). Step-cycle tests were performed on the dumbbell-shaped geometry to evaluate the energy dissipation and elasticity of the ICEs (three cycles have been carried out for each value of λ_{max}). Both the work of loading $w(\lambda_c)$ and the dissipated energy U_d per cycle were calculated by integrating the area under the stress-stretch curves as schematically described in Fig. S6. Then $U_d/w(\lambda_c)$ represents the dissipation ratio. The impedance of the ICEs was measured by alternating-current electrochemical impedance spectroscopy (EIS) on rectangular samples sandwiched between metal electrodes. The ionic conductivity was calculated based on the formula $\sigma = t/AR_b$, where *t* is the thickness of the sample, *A* is the contact area between the ICE and the electrode, and R_b is the bulk impedance extracted from the Nyquist plots on the interception of the real impedance Z' (Fig. S7).

Table 1 summarizes the mechanical properties including Young's modulus (*E*), strength (*s*), stretch at break (λ_b), fracture energy (Γ_c), and ionic conductivity (σ) of the P (MEA-*co*-IBA) (λ_0)-ICE(1). Several points can be made: The stretch at break λ_b is larger than 4 for all materials, a value that is amply sufficient for soft stretchable devices ($\lambda_b \geq 2$, or strain $\lambda_b \geq 100\%$)[50]. On the other hand, both strength and fracture energy at room temperature increase significantly with increasing pre-stretch (λ_0), demonstrating the stiffening and toughening effect of the MNE architecture by effectively delaying crack propagation. Note that the reference material with $\lambda_0 = 1$ is a more crosslinked analogue of the previously reported ICE[41] but with an added crosslinker and different monomer composition. Interestingly, the ICE samples with $\lambda_0 = 1.54$ and $\lambda_0 = 2.36$ exhibit roughly two orders of magnitude higher ionic conductivity at room temperature than that of the filler networks alone despite the lower lithium salt content (i.e., the LiTFSI content of the filler networks is approximately 10 wt% higher than that of the MNE according to Table S2–S3.

Figure 2a shows the comparison of the properties of P(MEA-*co*-IBA)(1)-ICE(1) and P(MEA-*co*-IBA)(2.36)-ICE(1), illustrating clearly the significant increase in stress at break, stiffness, fracture energy and ionic conductivity simultaneously. Such a simultaneous increase in properties has been a challenge in materials engineering along two lines. Specifically, stiffer materials (higher modulus *E*) tend to be less tough, and an increased ionic conductivity is associated with a higher segmental mobility[23,51,52] (i.e., a more liquid-like behavior). Therefore, a higher ionic conductivity generally comes at the expense of a lower fracture energy. Additionally, a similar behavior (but different values) is obtained on the samples that contain 0.5 M of LiTFSI in the precursor solutions of FNs named as P(MEA-*co*-IBA)(λ_0)-ICE(0.5). Details of the results can be found in Fig. S8 and Table S4. Figure 2b and Table S5 show the comparison of all the aforementioned properties of our system with those of previously reported state-of-the-art liquid-free

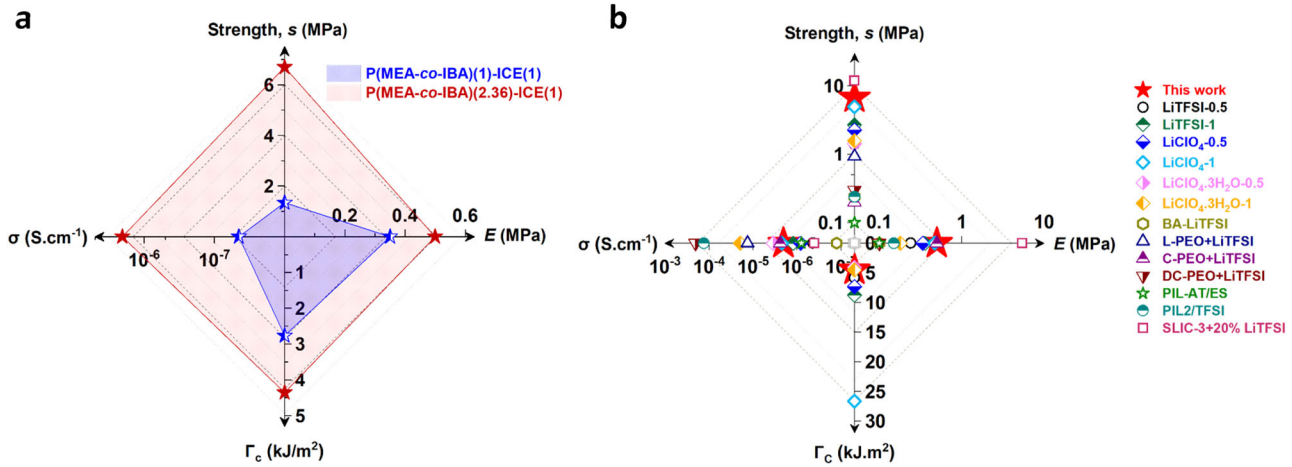

Fig. 2 | Comparative properties of ICEs based on simple and pre-stretched networks. a A comparison between the simple network P(MEA-*co*-IBA)(1)-ICE(1) and the MNE P(MEA-*co*-IBA)(2.36)-ICE(1) in terms of nominal stress at break (strength, *s*), stiffness (*E*), fracture energy (Γ_c) and ionic conductivity (σ). In this figure, ionic conductivity (*σ*) is plotted on a logarithmic axis, whereas strength (*s*), fracture energy (Γ_c), and Young's modulus (*E*) are plotted on linear axes. **b** Comparison between the MNE named P(MEA-*co*-IBA)(2.36)-ICE(1) and previously reported ionically conducting polymers with the same properties. In this figure, ionic conductivity (*σ*), Young's modulus (*E*), strength (*s*) are plotted on logarithmic axes, fracture energy (Γ_c) is plotted on a linear axis. The gray symbols at the center of the axes are the missing values of the corresponding samples. Details of the composition and actual values of the properties of the liquid-free ionic conductor samples used to plot Fig. 2b are provided in Table S5.

stretchable ionically conductive polymers[8,28,33–35,40–43]. Note that the reported MNEs are true elastomers in the sense of reversible elasticity with no residual deformation.

Although previously reported single polymer network based ionically conductive elastomers (ICEs) and supramolecular lithium ionic conductors (SLICs) can overcome these tradeoff issues and typically show very high toughness (up to 20 kJ/m^2 for ICEs and 29 MJ/m^3), they display significant residual deformation after unloading due to their large stretch at break ($\lambda_b > 14$ for ICEs and ($\lambda_b > 30$ for SLICs)[40,41]. However, P(MEA-*co*-IBA)(2.36)-ICE(1), containing only ~12 wt% of LiTFSI shows a fully reversible elasticity with a fracture energy $\Gamma_c \sim 5$ kJ/m^2 with a relatively low stretch at break ($\lambda_b \sim 4$). Additionally, while the SLICs containing 20% LiTFSI without plasticizers exhibit high strength (11.9 MPa) and stiffness (5.2 MPa), they show lower ionic conductivity ($4 \times 10^{-7}\ S.cm^{-1}$) at room temperature[40].

Remarkably the stiffening, strengthening and toughening mechanism of the ICEs with MNE architecture is very similar to that reported by E. Ducrot et al.[44] based on poly(ethyl acrylate) and poly(-methyl acrylate) but is quite different in nature from that of previously reported ionically conducting single network polymers[41]. In the ICE based on the MNE architecture, the presence of an embedded dilute and highly pre-stretched network introduces sacrificial bonds that can act as energy dissipators by bond scission and delay crack initiation, resulting in high stiffness, reversible elasticity, strength, and toughness. The high toughness in the previously reported single network ICEs originates from a high level of viscoelasticity due to both the interactions between the polymer chains and ions of the lithium salt and the very light crosslinking that leads to extreme stretchability. Furthermore, while the ionic conductivity of single network ICEs is markedly lithium salt-dependent, the ICEs with MNE architecture introduced in the current work show a high ionic conductivity with a much lower lithium salt content than the less conductive filler networks (Table S2).

Although the origins of increased mechanical properties and improved fracture resistance can be understood according to the pioneering studies on the multiple network elastomers[44] as discussed above, the mechanism for this significantly increased ionic conductivity is more subtle. As shown in Table S2, the samples of P(MEA-*co*-IBA)(1)-ICE(*x*), which are used as filler network ICEs contain ~30–35 wt% IBA. However, the weight percentage of IBA decreases to ~7–12 wt% in the samples of $\lambda_0 \sim 1.5$ and decreases to ~2–3 wt% for $\lambda_0 \sim 2.4$, hence the increased ionic conductivity may be related to the increased weight fraction of MEA. If this hypothesis is true, networks made from homopolymers P(MEA)(λ_0)-ICE(*x*) should show a higher ionic conductivity than those made from P(MEA-*co*-IBA)(λ_0)-ICE(*x*). To validate this hypothesis, we synthesized P(MEA)(λ_0)-ICE(1) networks by only using the monomer of MEA.

P(MEA)(1)-ICE(1) shows an ionic conductivity of $\sigma = 1.4 \times 10^{-6}\ S.cm^{-1}$ at 25 °C, two orders of magnitude higher than that of the P(MEA-*co*-IBA)(1)-ICE(*x*) of $\sigma = 4.5 \times 10^{-8}\ S.cm^{-1}$ at the same testing conditions and temperature. It is well-known that ion transport is governed by the Vogel–Fulcher–Tammann (VFT) relationship. The VFT equation predicts that a lower T_g in a polymer electrolyte leads to a higher ionic conductivity[53]. In the single networks, homopolymers of P(MEA) have a $T_g = -34$ °C, whereas the copolymers of the P(MEA-*co*-IBA) elastomers have a much higher $T_g = -5$ °C[54]; thus, the homopolymer P (MEA) is quite elastic, soft, and brittle, allowing for the easier transport of ions, while the copolymer P(MEA-*co*-IBA) is much more viscoelastic, strong, and tough. On the other hand, the single networks alone can hardly overcome the tradeoff between mechanical performance and ionic conductivity by simply tuning the monomer composition.

Comparing MNEs, with almost the same pre-stretch and LiTFSI content, P(MEA)(2.32)-ICE(1) exhibits a slightly higher ionic conductivity and strength than that of the P(MEA-*co*-IBA)(2.36)-ICE(1) at room temperature (Fig. 3a). Furthermore, the strength increases as a function of Young's modulus (Fig. S9) and is comparable to that of P(MEA-*co*-IBA)(2.36)-ICE(*x*), illustrating the feasibility of making strong and tough ICEs with reasonable ionic conductivity and mechanical properties from homopolymers of P(MEA) based on the MNE architecture.

It has been argued that the ionic conductivity of the polymer electrolytes can be improved by lowering the T_g of the polymer[55–57]. Unfortunately, reducing the T_g can be deleterious to the mechanical performance[58]. Interestingly, as shown in Fig. 3b, for the P(MEA-*co*-IBA)(λ_0)-ICE(*x*) family, the strength and stiffness can be increased simultaneously in spite of the significant decrease of the T_g (Fig. S10), overcoming the tradeoff between ionic conductivity and mechanical properties. Note that the nominal stress-stretch curves of the ICEs synthesized from the filler network can be rescaled as nominal stress at

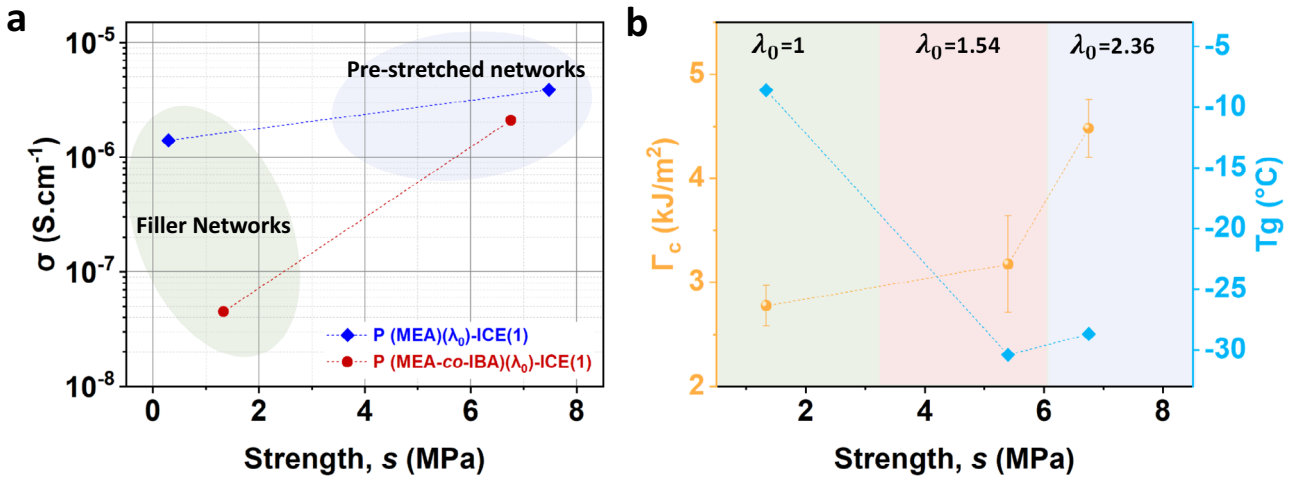

Fig. 3 | Ionic conductivity, strength, and toughness of ICEs with varying pre-stretched networks. a Ionic conductivity σ versus stress at break (i.e., strength, s) of the P(MEA-*co*-IBA)(λ_0)-ICE(1) and homopolymers of P(MEA)(λ_0)-ICE(1); samples with the pre-stretch of $\lambda_0 = 1$ and $\lambda_0 = 2.36$ is used for the ICEs based on P(MEA-*co*-IBA)(λ_0)-ICE(1), while $\lambda_0 = 1$ and $\lambda_0 = 2.32$ for the ICEs based on P(MEA)(λ_0)-ICE(1). **b** Toughness versus strength of the P(MEA-*co*-IBA)(λ_0)-ICE(1) with different pre-stretched networks (λ_0) and T_g. Note that the samples with pre-stretched networks show and increased toughness and strength despite of significant decrease in T_g. A minimum of three samples were tested for each data point to measure toughness and strength, with error bars representing the standard deviation (SD).

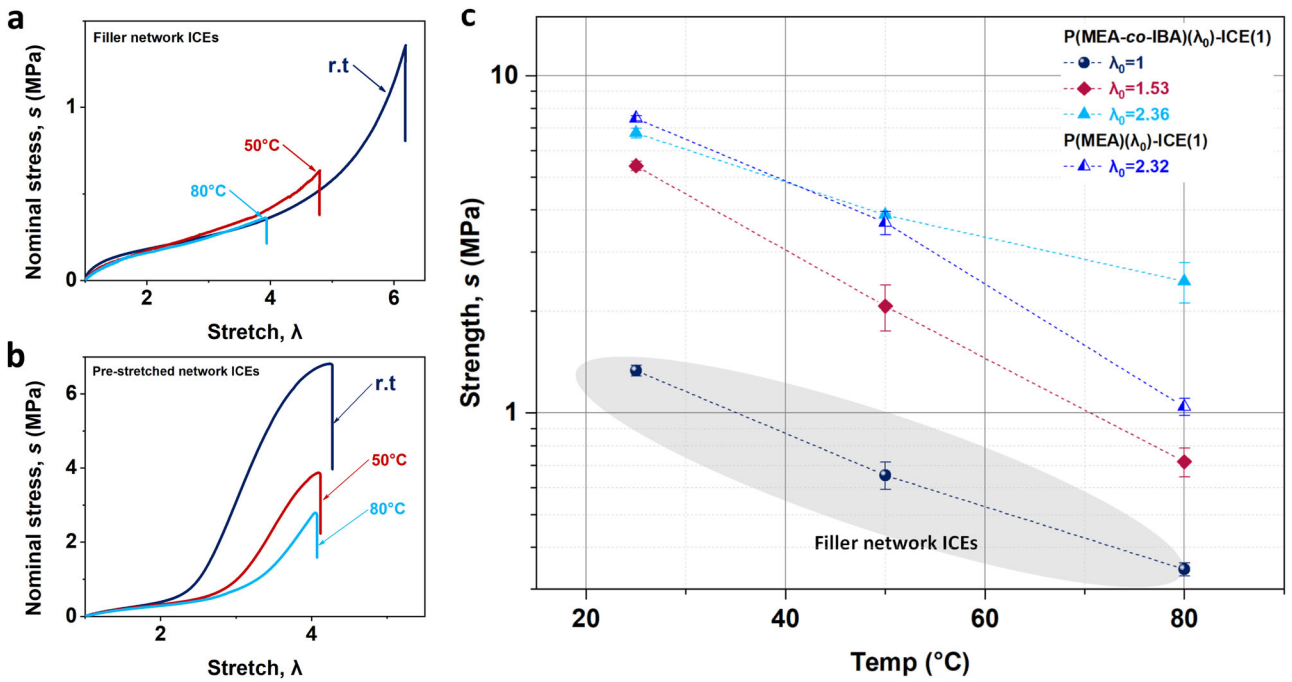

Fig. 4 | Mechanical properties of the ICEs at different temperatures tempera-tures. a, **b** Nominal stress vs stretch curves of the P(MEA-*co*-IBA)(1)-ICE(1), and P(MEA-*co*-IBA)(2.36)-ICE(1). **c** Strength of the P(MEA-*co*-IBA)(λ_0)-ICE(1) and P(MEA)(2.32)-ICE(1) over temperatures. A minimum of three samples were tested for each data in Fig. 4c, with error bars representing the standard deviation (SD). Note that for some data points in Fig. 4c, error bars are not visible because they are smaller than the marker size.

break as a function of $\lambda^*\lambda_0$ (Figs. S11–S12) as previously reported for an acrylate MNE[45].

Among the nine groups of samples categorized as P(MEA-*co*-IBA)(λ_0)-ICE(x) and P(MEA)(λ_0)-ICE(1) series, the $\lambda_0 = 2.36$ sample exhibited the highest fracture energy, strength, and high ionic conductivity, primarily due to low T_g. Based on the MNEs synthesized from ethyl acrylate monomers[45], even higher Young's moduli can be expected with $\lambda_0 \geq 2.36$, while maintaining high ionic conductivity. However, increasing λ_0 further may lead to a decrease in strength and no benefit in toughness.

Uniaxial tensile tests were also performed at higher temperatures, on the ICEs based on copolymers of P(MEA-*co*-IBA) and homopolymers of P(MEA). Figure 4a shows that P(MEA-*co*-IBA)(1)-ICE(1) (i.e., ICEs used as filler networks) loses extensibility significantly at 50 °C and 80 °C, presumably because of the decrease in viscoelastic dissipation. On the other hand, the MNE including P(MEA-*co*-IBA)(1.53)-ICE(1), and P(MEA-*co*-IBA)(2.36)-ICE(1) with higher pre-stretched network strands show a much less pronounced decrease in stretch at break with temperature (Figs. 4b, S13). Moreover, P(MEA-*co*-IBA)(2.36)-ICE(1) shows higher mechanical performance than P(MEA-*co*-IBA)(1.53)-ICE(1), indicating

https://doi.org/10.1038/s41467-024-55472-8

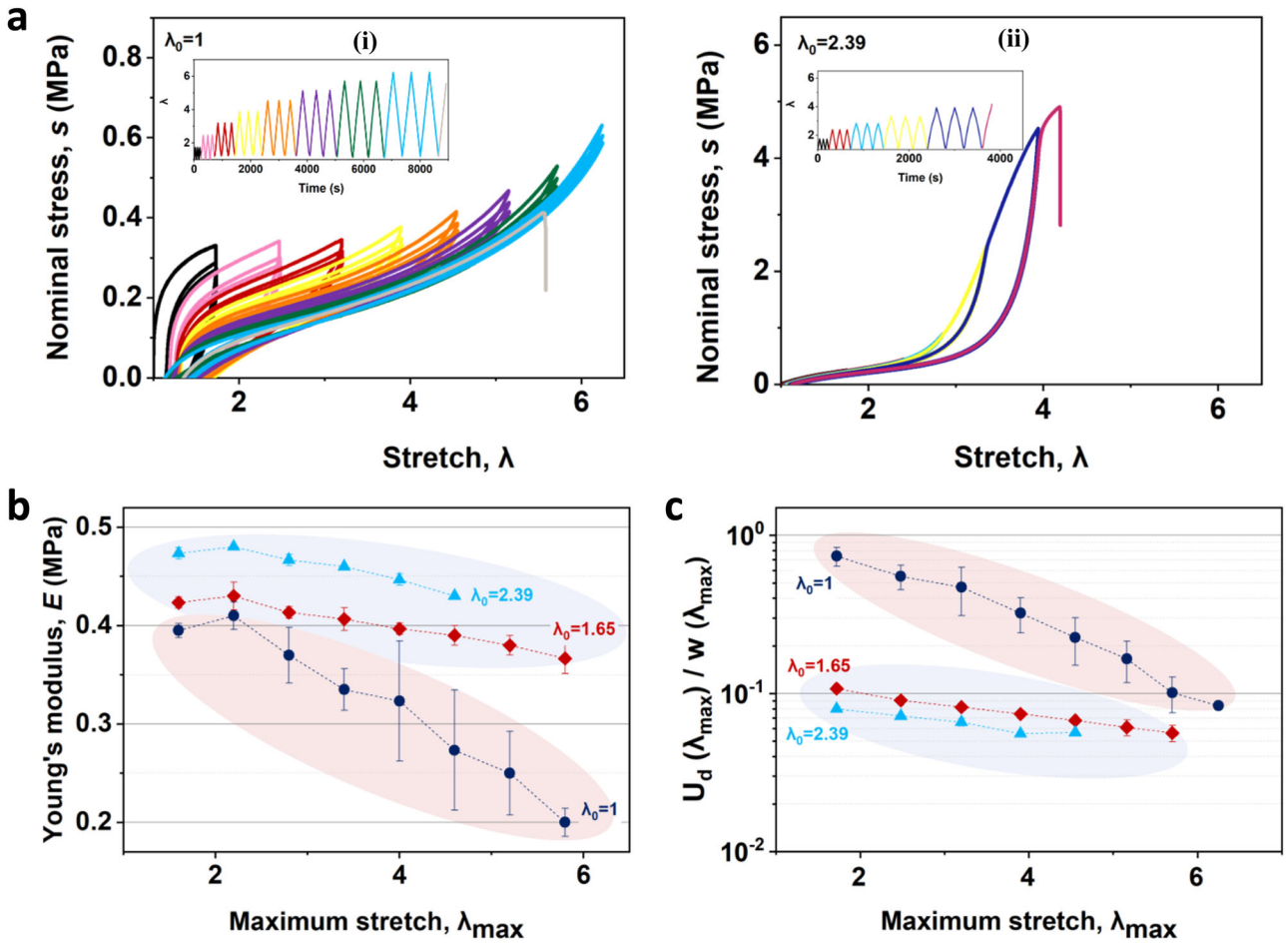

Fig. 5 | Step-cycle Loading-unloading Curves of the ICEs with Different λ_0. **a** Nominal stress-stretch curves of a P(MEA-*co*-IAB)(λ_0)-ICE(1) with different pre-stretch; (i) $\lambda_0 = 1$ represents the filler network with a markedly viscoelastic character; whereas (ii) is the pre-stretched networks of P(MEA-*co*-IBA)(2.39)-ICE(1). Three cycles were applied for each strain; a fixed displacement rate of 500 μm/s was applied for all the samples, resulting in a stretch rate of ~0.09/s. **b** Evolution of the loading modulus measured during cycles. **c** Corresponding hysteresis ratio in the third cycle of the ICEs with different pre-stretch. $U_d(\lambda_{max})$ is the dissipated energy per cycle and $w(\lambda_{max})$ is the total work of loading at a given stretch λ_{max}, $U_d(\lambda_{max})/w(\lambda_{max})$ provides insight into the energy dissipation efficiency of the ICEs. A minimum of three samples were tested for each data points in figure **b**, **c**; error bars represent SD. Note that for some data points in Figs. 5b and 5c, error bars are not visible because they are smaller than the marker size.

that the higher pre-stretch leads to better temperature-resistance as previously found for MNE based on acrylates[46].

The samples of P(MEA)(2.32)-ICE(1) also show a negligible drop in stretch at break (Fig. S14). The evolution of mechanical strength of the samples with temperature is summarized in Fig. 4c. All the ICEs based on the MNE architecture possess a significantly higher strength than the single network ICEs (i.e., the gray area on the plot) at the same temperature. Interestingly, P(MEA-*co*-IBA)(2.36)-ICE(1) possess higher strength than P(MEA)(2.32)-ICE(1), illustrating that the ICEs based on copolymers of P(MEA-*co*-IBA) still have better temperature-resistance than the ICEs based on the homopolymers of P(MEA) with almost the same λ_0.

It is worth mentioning that the $\lambda_0 = 2.36$ sample exhibits exceptional strength at 80 °C. This aligns with the toughening mechanisms described in Slootman's[46] work on multiple network elastomers (MNEs) synthesized from ethyl acrylate and methyl acrylate monomers, where pre-stretched filler networks enhance fracture energy and mechanical strength through diluting highly pre-stretched strands and creating a large damage zone that absorbs energy and prevents crack propagation. At 80 °C, the toughening in the $\lambda_0 = 2.36$ sample is driven primarily by this mechanism, independent of viscoelastic dissipation. However, further increasing λ_0 may not proportionally enhance strength because of the concomitant effect of diluting the filler network.

Figures 5a and S15 show the step-cycle experiments under increasing stretch λ_{max} performed on the P(MEA-*co*-IBA)(λ_0)-ICE(1). All the ICE samples (with different λ_0) synthesized from the copolymer network structures of P(MEA-*co*-IBA) show larger hysteresis loops in the first cycle than in the second and third cycles, illustrating a mechanism of energy dissipation involving damage in the first cycle. However, the origin of the energy-dissipating mechanism for the ICEs with different λ_0 is different. In the original network ICEs with $\lambda_0 = 1$ (i.e., Fig. 5a (i)), the strain rate dependent energy dissipation mechanism is due to damage and viscoelasticity, quite similar to that of single network ICEs reported by Yiming et al.[41]. However, the strain-dependent irreversible breakage of sacrificial bonds in the pre-stretched networks is the dominant energy dissipation mechanism in the highly pre-stretched ICEs[44]. Different dominant energy dissipation mechanisms, i.e., viscoelastic dissipation in the single network ICEs and bond scission dissipation in the MNEs, lead to significantly different mechanical performance. For example, a negligible drop in Young's modulus with cycling at increasing λ_{max} was observed in the ICEs with MNE architecture ($\lambda_0 = 1.65$ and $\lambda_0 = 2.39$), while there is a dramatic drop in Young's modulus of the filler networks alone (Fig. 5b). Additionally, the ICE with MNE architecture shows a relatively low dissipation ratio (i.e., <10%) than that of the original samples (i.e., ~18%) at similar stretches (Fig. 5c). Moreover, MNEs exhibit relatively

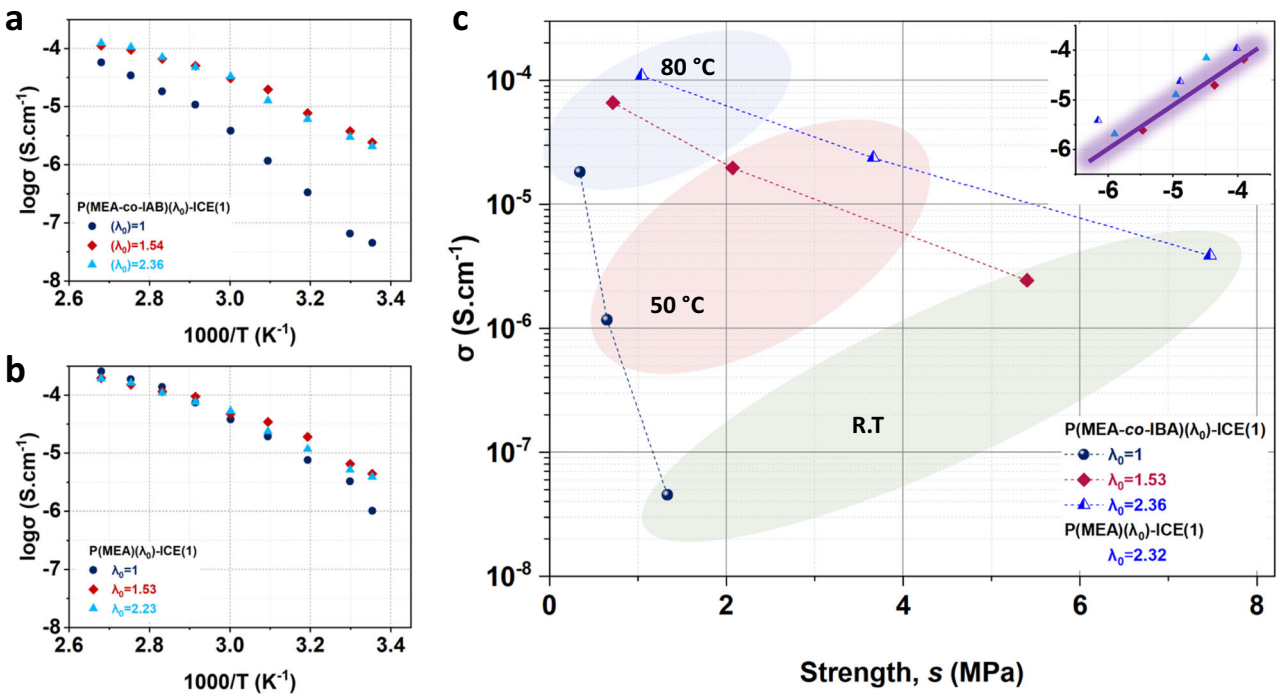

Fig. 6 | Electrical Properties of the ICEs at different temperatures. **a**, **b** Temperature dependence of the ionic conductivity of the ICEs tested on the samples of P(MEA-*co*-IBA)(λ_0)-ICE(1) and P (MEA)(2.32)-ICE(1). **c** Plot of ionic conductivity versus strength of ICEs at various temperatures, based on different pre-stretched networks and MNE architectures. Inset: The logarithm of ionic conductivity as a function of $-(11+s)/3$. Notably, the data for pre-stretched networks align along a straight line, which can be described by the formula $\log\sigma = -(11+s)/3$. This indicates that as temperature increases, ionic conductivity rises while strength decreases.

constant hysteresis ratios across different pre-stretch levels, while the filler networks show a significant reduction in hysteresis ratios as the maximum stretch increases. As a result, the single network ICEs are more susceptible to fatigue, and using these ICEs under cyclic deformation can be challenging, whereas the ICEs with MNE architecture are elastic and can resist many cycles of deformation[26].

Ionic Conductivity

Electrochemical impedance spectroscopy (EIS) scans were performed at frequencies varying between 0.1 Hz and 10 MHz and temperatures increasing from 25 °C to 100 °C. Based on the EIS results and data analysis, the imaginary impedance Z'' was plotted as a function of real impedance Z' and the impedance magnitude $|Z|$ and phase angle were plotted as a function of frequency. The corresponding plots at 30 °C are shown in Figs. S16–18.

Based on the EIS measurements, ionic conductivities were calculated from the Nyquist plots and are plotted as a function of temperature (Fig. 6a, b; Fig. S19). At room temperature, P(MEA-*co*-IBA)(1)-ICE(1) (i.e., filler networks of copolymers with a pre-stretch $\lambda_0 = 1$) exhibit a much lower ionic conductivity than that of their pre-stretched counterparts (i.e., $\lambda_0 = 1.53$, $\lambda_0 = 2.36$) and become more similar at higher temperatures (Fig. 6a). This is most likely due to differences in monomer composition (only MEA is used for the matrix networks) and hence in glass transition temperature. As the temperature increases, all materials exhibit reduced viscoelasticity at $T \gg T_g$, which leads to a similar ionic conductivity behavior due to increased segmental mobility. Replacing copolymers of P(MEA-*co*-IBA) with homopolymer networks of P(MEA) increases ionic conductivity, probably because of the higher concentration of conductive ether groups in the homopolymer and the lower glass transition temperature (i.e., $T_g = -34$ °C)[54].

When plotting the ionic conductivity as a function of $T - T_g$ (Fig. S20a), we observed that the P(MEA-*co*-IBA)(2.36)-ICE(1) consistently exhibits slightly higher ionic conductivity than that of P(MEA-*co*-IBA)(1)-ICE(1) at elevated temperatures. Additionally, as highlighted in Fig. S20b, which represents the ionic conductivity as function of λ_0 at 58 °C (dark blue area), 68 °C (red area), and 98 °C (light blue area) above their T_g, the P(MEA-*co*-IBA)(2.36)-ICE(1) consistently exhibits slightly higher ionic conductivity than P(MEA-*co*-IBA)(1)-ICE(1) at the same $T - T_g$. This suggests that the pre-stretch can affect the ionic conductivity; however, this effect is relatively minor—less than a factor of two at temperatures significantly above T_g.

Both ionic conductivity and mechanical properties are affected by temperature, and both these parameters are equally important when high-temperature applications are considered. Therefore, we plot ionic conductivity as a function of strength at different temperatures for the ICEs with different λ_0 and polymer compositions (Fig. 6c, Table S6). The MNE of P (MEA-*co*-IBA)(λ_0)-ICE(1) with $\lambda_0 = 1.54$ and $\lambda_0 = 2.36$ exhibit higher strength and ionic conductivity than the single network ICEs with $\lambda_0 = 1$; From Fig. 6c, it is clear that the samples with relatively high pre-stretch of $\lambda_0 = 2.36$ lead to a better combination of strength and ionic conductivity in the P(MEA-*co*-IBA)(λ_0)-ICE(1) family. Comparing the copolymer-based ICE named P(MEA-*co*-IBA)(2.36)-ICE(1) and homopolymer-based ICE named P(MEA)(2.32)-ICE(1) with almost similar values of λ_0, the $\lambda_0 = 2.32$ sample based on homopolymers have a slightly higher ionic conductivity and a much lower strength than the $\lambda_0 = 2.36$ sample based on copolymers at 50 °C and 80 °C. In conclusion, the copolymer based ICEs display the best compromise between ionic conductivity and strength at higher temperatures (i.e., 50 °C and 80 °C), while at room temperature it is the P(MEA)(2.32)-ICE(1) that has the best compromise. In general, both the pre-stretch λ_0 and the monomer compositions (i.e., homopolymer or copolymers) should be considered for the optimization of properties.

While the P(MEA)(2.32)-ICE(1) shows higher strength, stiffness, and ionic conductivity at room temperature, the corresponding copolymer based MNEs outperforms the homopolymer in several aspects. First, the MNE based on the copolymer demonstrates a higher

stretch at break than the MNE based on the homopolymer (Fig. S11). Second, in moderately pre-stretched networks, copolymers show higher stress, stretch at break, and fracture toughness compared to homopolymers, while maintaining comparable ionic conductivities. Third, in highly pre-stretched networks, copolymers show higher strength than homopolymers at high temperatures.

In this study, by using the binary mixtures of a low T_g monomer MEA, a high T_g monomer IBA, and a dry lithium salt LiTFSI, we have developed a family of ionically conductive elastomers based on the MNE architecture. Our MNE structure relies on sacrificial bonds for strength and an embedded pre-stretched network for stiffness, while maintaining high segmental mobility due to low T_g polymers. This combination results in a high toughness and very low residual deformation upon unloading as well as a good ionic conductivity around 10^{-6} S/cm near room temperature. Preferential breakage of the bonds in the filler networks at higher strains can dissipate a large amount of energy, leading to high toughness, while the same pre-stretched network greatly increases the reversibility of the elasticity in agreement with previous investigations on the MNEs[44,45]. This leads to excellent fatigue resistance[26,59], making the material suitable for cyclic loads over long times. In summary, the resultant ionically conducting MNEs combine a behavior typical of tough elastomers in terms of Young's moduli, strength, and toughness, with a reasonable ionic conductivity at room temperature.

This family of stretchable lithium ionic conductors are promising for stretchable ionotronic devices based on safe solid electrolytes without the hassles of liquid-leakage-related issues[1,2] and in particular for wearables devices and bioelectronics with direct contact with human tissue, thanks to the low-toxic nature of P(MEA) (approved by the FDA) and its excellent blood compatibility[60]. Last not but least, the ICEs have a strong potential to be used as polymer electrolytes in lithium-ion batteries. Although their modulus may not be high enough to prevent dendrite growth when Li-metal electrodes are used, the several kJ/m^2 toughness may be valuable.

Methods

Materials

All the chemicals [ethylene glycol methyl ether acrylate (MEA) and isobornyl acrylate (IBA) as monomers, bistrifluoromethanesulfonimide lithium salt (LiTFSI) as electrolyte salt, poly (ethylene glycol diacrylate) (PEGDA) with a molecular weight of M_n = 250 g/mol as crosslinker and 2-hydroxy-2-methylpropiophenone (HMP) as UV initiator] were purchased from Sigma Aldrich. The monomers MEA and IBA were purified over a column of activated alumina to remove the inhibitor before use.

Generalities of Network Synthesis

The synthesis of ICEs with various values of pre-stretch λ_0 was carried out in a glove box (Mbraun Unilab) under a nitrogen atmosphere to avoid side reactions with the oxygen and moisture in the air. Before being introduced into the glovebox, the monomers of MEA and IBA, UV initiator HMP, and the crosslinker PEGDA were bubbled with nitrogen for a minimum of 30 min to remove the dissolved oxygen. All the samples were stored in the glove box to avoid moisture absorption due to the presence of lithium.

Synthesis of the Filler Network

The synthesis follows the procedure reported by Yiming et al.[41] but with added crosslinker to obtain ICEs with densely crosslinked networks, whereas no crosslinker was used in the previous works of Yiming et al.[41]. The filler networks were synthesized by UV free radical copolymerization of solutions of MEA and IBA (30 mol% of IBA relative to MEA monomer), LiTFSI as electrolyte salt (molar concentrations being controlled at either 0.5 M or 1 M), PEGDA as crosslinker (0.5 mol % relative to the total molar concentration of monomers), and HMP as a UV initiator (1.16 mol% relative to the total molar concentration of monomers). First, the electrolyte salt LiTFSI was dissolved in the MEA monomer by stirring for 5 min, and then the monomer IBA, HMP, and PEGDA were added to obtain the precursor solutions. The reactants were stirred for 5 min to obtain homogeneous precursor solutions before being injected in a 1 mm thick glass mold. As shown in Fig. S1, the mold was composed of two glass plates covered with transparent PET films (with a hydrophobic surface), with a silicone spacer to control the sample thickness (~0.7–0.9 mm) and two metal frames to seal the mold. The mold was placed under UV (λ = 365 nm) for two hours. The UV power was kept low (below 10 μW·cm^{-2}) to induce a slow polymerization in order to decrease the number of simultaneous growing chains and the number of termination reactions. Transparent filler networks were obtained after 2 h of UV curing. Samples of ICEs made from only MEA were also synthesized with variable concentrations of LiTFSI and using the same amount of PEGDA and HMP. As described in Table S1, approximately 1.5 wt% weight loss due to the unreacted monomers were estimated.

Note that the degree of crosslinking of the filler network is an important factor affecting the onset of strain hardening of multiple network elastomers, and mechanical properties change accordingly. However, samples used in this work were synthesized independently in each step and UV polymerization does not result in perfectly reproducible degrees of crosslinking. This in turn affects the equilibrium swelling (λ_0). When we plot the nominal stress at break as a function of $\lambda^*\lambda_0$ for resultant MNE, where λ is the stretch, we can see that the strain hardening occurs at a different value of $\lambda^*\lambda_0$ that depends on the equilibrium degree of swelling of the filler networks. Hence every prepared single network leads to a slightly different value of pre-stretch (λ_0) of the MNE due to the experimental reproducibility. We provide the pre-stretch (λ_0) for each sample and error bar (if needed) that has been tested. It is crucial to prepare all samples from the same initial networks to ensure identical pre-stretch. However, due to the extensive characterizations required for a full understanding of these materials, not all samples in this study were derived from the same filler networks. Estimating the exact amount of material needed for testing was challenging, necessitating independent synthesis at each step.

Synthesis of Matrix Networks

The synthesis method of the MNE used is inspired by the previously published work of Chen et al.[47]. Filler networks made from the salt-containing copolymers P(MEA-co-IBA) were swollen for 7 and 9 h for the second and third swelling steps at approximately 13–15 °C in a solution of MEA monomer containing 0.5 M LiTFSI, 0.01 mol% crosslinker PEGDA, and 0.01 mol% UV initiator HMP relative to the MEA in the swelling bath. The swelling time was determined based on weight gain measurements during swelling. If the swelling time is too long, the solution in the swelling bath may start to polymerize while if the swelling time is too short, the samples do not reach equilibrium. We typically use the longest swelling time that does not trigger polymerization and check that the mass gain is negligible at this stage.

Notably, networks created using only the MEA monomer reach equilibrium faster than those based on MEA and IBA solutions at the same swelling temperature. Therefore, P(MEA) networks were swollen for 5 and 7 h for the second and third swelling steps under the same conditions and with the same amounts of MEA monomer, crosslinker PEGDA, and UV initiator HMP as used for the copolymers.

The swollen piece of the ICE network was taken out of the bath clamped between PET sheets and tightened between glass plates. The polymerization was conducted in a similar way as for the filler network ICEs. The synthesis can be repeated multiple times through several swelling and polymerization steps resulting in the formation of multiple network elastomers (MNE). In this work, we performed a maximum of two swelling and polymerization steps.

The fraction of the FN ϕ_{FN} was determined based on the Eq. (2),

$$\phi_{FN} = \frac{V_{FN}}{V_{MN}} = \frac{m_{FN}}{m_{MN}} \times \frac{\rho_{MN}}{\rho_{FN}} = \frac{1}{\left(\lambda_0^3\right)} \quad (2)$$

Where V_{FN} is the volume of filler networks, V_{MN} is the volume of the multiple networks, m_{FN} and m_{MN} are the weight of the filler and multiple networks, ρ_{FN} and ρ_{MN} are the density of the filler and multiple networks, and λ_0 is the pre-stretch of the filler networks.

Characterization of water uptake

As-prepared, liquid-free P(MEA-co-IAB)(λ_0)-ICE(1) samples, each with varying initial λ_0 values, were stored under ambient conditions. The weight of each sample was measured at regular intervals: every 2 h during the first day, every 5–6 h on the second day, and every 1–12 h thereafter. This monitoring continued for a total period of 92 h to track weight changes over time.

Mechanical tests

Mechanical tests were performed on a standard tensile Instron machine, model 5565, using a 100 N load cell. A video extensometer gave a local measurement of the stretch λ = L/L0, where L0 is the initial gauge length (Fig. S4). Specimens were cut into a dumbbell shape using a normalized cutter (central part: length 20 mm, cross-section 4 mm, and thickness 0.9–2.2 mm depending on the sample). Uniaxial tensile tests from small to large strains were performed at a constant velocity of the crosshead of 500 μm s^{-1} and the typical initial strain rate on the central part of the sample was around 0.09 s^{-1}. Using the nominal stress and strain, Young's modulus E was calculated at a strain of ~20%. Nominal stress was defined as the tensile force per unit of initial area using the following Eq. (3):

$$s = F/w.h \quad (3)$$

F, w and h being measured force, width, and thickness of the samples.

Determination of the fracture energy Γ_c

Fracture tests were performed using the classical single edge notch test (Fig. S5) on an Instron testing machine. Each tested sample had a width (w_0) of 5 mm and the thickness depends on the sample itself between 0.9 mm and 2.2 mm. The sample was fixed between clamps previously spaced L = 20 mm. The pre-cut sample was prepared by using a razor blade and had a 1 mm-long single-edge notch that was measured specifically for each sample. The uncut sample was stretched for the measurement of the force-distance curve. Samples were dotted with white paint to allow a measurement of the local elongation via the video extensometer. Force and elongation were measured while deforming the sample by moving the crosshead at 500 μm s^{-1}, corresponding to a nominal strain rate of 0.16 s^{-1}. The fracture energy (Γ_c) is calculated by using the Greensmith approximation (Eq. 4):

$$\Gamma_c = 6.w.c/\sqrt{\lambda_c} \quad (4)$$

with c the length of the crack, λ_c the strain at break in single edge notch experimental, and w the strain energy density calculated by integration of the stress versus engineering strain of un-notched samples, until $\varepsilon_c\left(\varepsilon_c = \lambda_c - 1\right)$.

Step cycle experiments

Incremental loading and unloading cycles were performed with the same experimental setup as the tensile tests at a crosshead speed of 500 μm.s^{-1}, corresponding to a stretch rate of 0.09s^{-1}. Cycles were applied between nearly λ = 1.7 to λi. Three cycles were performed at each value of maximum stretch then the maximum of λ was incremented (λi + 0.7 > λi) and three cycles were performed again. The strain ratio (λ) measured by video extensometer, was recorded during the experiments. The calculation of hysteresis U_d under loading-unloading cycles and the work $w(\lambda_c)$ done by the loading only is described schematically in Fig. S6. The ratio of U_d/W indicates the dissipation ratio.

Electrochemical Impedance Spectroscopy (EIS) measurements

Impedance tests were performed with an electrochemical impedance spectroscopy (a Modulab Solartron Analytical potentiostat (Ametek, Berwyn, Pennsylvania, USA) with a FRA 1 MHz frequency analyser module, over a frequency range of 10 MHz to 0.1 Hz (11 points per decade) and an amplitude of 30 mV. A rectangular strip of the sample was prepared by using a cutter. To make the electrode, a thin silver paste layer was homogeneously coated on the surface of the sample, and then a conductive copper tape was adhered on top to connect the potentiostat via a cable as shown in Fig. S7. We extract the bulk resistance R_b from the Nyquist plots. The ionic conductivity was calculated from $\sigma = t/AR_b$, where t corresponds to the thickness of the sample and A corresponds to the effective overlap area (the area covered by the electrode). Note that all the samples were stored in the glovebox before performing EIS experiments, and the experiments were completed in minutes to minimize the effect of ambient moisture on the results.

Data availability

The data presented in the main paper and supplementary information is deposited in https://entrepot.recherche.data.gouv.fr/dataverse/psl with the https://doi.org/10.57745/RGBMNP. All data are also available from the corresponding author upon request.

References

1. Park, J. M., Lim, S. & Sun, J. Y. Materials development in stretchable iontronics. *Soft Matter* **18**, 6487–6510 (2022).
2. Yang, C. & Suo, Z. Hydrogel ionotronics. *Nat. Rev. Mater.* **3**, 125–142 (2018).
3. Niu, W. & Liu, X. Stretchable ionic conductors for soft electronics. *Macromol. Rapid Commun.* **43**, e2200512 (2022).
4. Mackanic D. G., Kao M. & Bao Z. Enabling deformable and stretchable batteries. *Adv. Energy Mater.* **10**, 2001424 (2020).
5. Chen, X., Huang, H., Pan, L., Liu, T. & Niederberger, M. Fully integrated design of a stretchable solid-state lithium-ion full battery. *Adv. Mater.* **31**, e1904648 (2019).
6. Wirthl, D. et al. Instant tough bonding of hydrogels for soft machines and electronics. *Sci. Adv.* **3**, e1700053 (2017).
7. Luo, Z., Li, W., Yan, J. & Sun, J. Roles of ionic liquids in adjusting nature of ionogels: a mini review. *Adv. Funct. Mater.* **32**, https://doi.org/10.1002/adfm.202203988 (2022).
8. Yiming, B. et al. Ambiently and mechanically stable ionogels for soft ionotronics. *Adv. Funct. Mater.* **31**, 2102773 (2021).
9. Shi, L. et al. Highly stretchable and transparent ionic conductor with novel hydrophobicity and extreme-temperature tolerance. *Research* **2020**, 2505619 (2020).
10. Cao, Z., Liu, H. & Jiang, L. Transparent, mechanically robust, and ultrastable ionogels enabled by hydrogen bonding between elastomers and ionic liquids. *Mater. Horiz.* **7**, 912–918 (2020).
11. Zhang, L. M. et al. Self-healing, adhesive, and highly stretchable ionogel as a strain sensor for extremely large deformation. *Small* **15**, e1804651 (2019).
12. Lei, Z. & Wu, P. A highly transparent and ultra-stretchable conductor with stable conductivity during large deformation. *Nat. Commun.* **10**, 3429 (2019).

13. Ding, Y. et al. Preparation of high-performance ionogels with excellent transparency, good mechanical strength, and high conductivity. *Adv. Mater.* **29**, https://doi.org/10.1002/adma.201704253 (2017).
14. Wang, M. et al. Tough and stretchable ionogels by in situ phase separation. *Nat. Mater.* **21**, 359–365 (2022).
15. Li, W. et al. Supramolecular Ionogels tougher than metals. *Adv. Mater.* **35**, 2301383 (2023).
16. Ren, Y. et al. Ionic liquid–based click-ionogels. *Sci. Adv.* **5**, eaax0648 (2019).
17. Kamio, E., Yasui, T., Iida, Y. & Gong, J. P. Inorganic/organic double-network gels containing ionic liquids. *Adv. Mater.* **29**, 1704118 (2017).
18. Zhang, M. et al. Mechanically robust and highly conductive ionogels for soft Ionotronics. *Adv. Funct. Mater.* **33**, https://doi.org/10.1002/adfm.202208083 (2022).
19. Kim, Y. M. & Moon, H. C. Ionoskins: nonvolatile, highly transparent, ultrastretchable ionic sensory platforms for wearable electronics. *Adv. Funct. Mater.* **30**, 1907290 (2020).
20. Creton, C. 50th anniversary perspective: networks and gels: soft but dynamic and tough. *Macromolecules* **50**, 8297–8316 (2017).
21. Persson, B. N. J., Albohr, O., Heinrich, G. & Ueba, H. Crack propagation in rubber-like materials. *J. Phys. Condens. Matter* **17**, R1071–R1142 (2005).
22. Gent, A. N. Adhesion and strength of viscoelastic solids. Is there a relationship between adhesion and bulk properties. *Langmuir* **12**, 4492–4496 (1996).
23. Jones, S. D., Schauser, N. S., Fredrickson, G. H. & Segalman, R. A. The role of polymer–ion interaction strength on the viscoelasticity and conductivity of solvent-free polymer electrolytes. *Macromolecules* **53**, 10574–10581 (2020).
24. Bamford, J. T. et al. Improved mechanical strength without sacrificing li-ion transport in polymer electrolytes. *ACS Macro Lett.* **13**, 638–643 (2024).
25. Bai, R., Yang, J. & Suo, Z. Fatigue of hydrogels. *Eur. J. Mech. A-Solids* **74**, 337–370 (2019).
26. Gabriel, E. et al. is mechanical fatigue different from toughness in elastomers? The role of damage by polymer chain scission. *Sci. Adv.* **7**, eabg9410 (2021).
27. Seo, D. G. & Moon, H. C. Mechanically robust, highly ionic conductive gels based on random copolymers for bending durable electrochemical devices. *Adv. Funct. Mater.* **28**, 1706948 (2018).
28. Shi, L. et al. Highly stretchable and transparent ionic conducting elastomers. *Nat. Commun.* **9**, 2630 (2018).
29. Wang, W. et al. Strong and highly stretchable ionic conductive elastomer based on hydrogen bonding. *Compos. Sci. Technol.* **201**, https://doi.org/10.1016/j.compscitech.2020.108559 (2021).
30. Shi, P., Wang, Y., Wan, K., Zhang, C. & Liu, T. A waterproof ion-conducting fluorinated elastomer with 6000% stretchability, superior ionic conductivity, and harsh environment tolerance. *Adv. Funct. Mater.* **32**, 2112293 (2022).
31. Xu, Z., Li, R., Li, H., Gao, G. & Chen, T. Flexible and adhesive liquid-free ionic conductive elastomers toward human-machine interaction. *Soft Matter* **18**, 7103–7111 (2022).
32. Luo, C. et al. A fully self-healing and highly stretchable liquid-free ionic conductive elastomer for soft ionotronics. *Adv. Funct. Mater.* **33**, 2304486 (2023).
33. Zhang, P. et al. Dynamically crosslinked dry ion-conducting elastomers for soft iontronics. *Adv. Mater.* **33**, e2101396 (2021).
34. Qu, X. et al. Solid-state and liquid-free elastomeric ionic conductors with autonomous self-healing ability. *Mater. Horiz.* **7**, 2994–3004 (2020).
35. Kim, H. J., Chen, B., Suo, Z. & Hayward, R. C. Hayward. Ionoelastomer junctions between polymer networks of fixed anions and cations. *Science* **367**, 773–776 (2020).
36. Li, X., Liu, J., Guo, Q., Zhang, X. & Tian, M. Polymerizable deep eutectic solvent-based skin-like elastomers with dynamic schemochrome and self-healing ability. *Small* **18**, e2201012 (2022).
37. Wang, M. et al. Multifunctional liquid-free ionic conductive elastomer fabricated by liquid metal induced polymerization. *Adv. Funct. Mater.* **31**, https://doi.org/10.1002/adfm.202101957 (2021).
38. Li, R. et al. Autonomous self-healing, antifreezing, and transparent conductive elastomers. *Chem. Mater.* **32**, 874–881 (2020).
39. Li, R. et al. Highly transparent, self-healing conductive elastomers enabled by synergistic hydrogen bonding interactions. *Chem. Eng. J.* **393**, https://doi.org/10.1016/j.cej.2020.124685 (2020).
40. Yiming, B. et al. Decoupling of mechanical properties and ionic conductivity in supramolecular lithium ion conductors. *Nat. Commun.* **10**, 5384 (2019).
41. Yiming, B. et al. A mechanically robust and versatile liquid-free ionic conductive elastomer. *Adv. Mater.* **33**, e2006111 (2021).
42. Yiming, B. et al. Molecular mechanism underpinning stable mechanical performance and enhanced conductivity of air-aged ionic conductive elastomers. *Macromolecules* **55**, 4665–4674 (2022).
43. Yiming, B. et al. Designing ionic conductive elastomers using hydrophobic networks and hydrophilic salt hydrates with improved stability in air. *Adv. Electron. Mater.* **9**, 2300069 (2023).
44. Ducrot, E., Chen, Y., Bulters, M., Sijbesma, R. P. & Creton, C. Toughening elastomers with sacrificial bonds and watching them break. *Science* **344**, 186–189 (2014).
45. Millereau, P. et al. Mechanics of elastomeric molecular composites. *Proc. Natl Acad. Sci. USA* **115**, 9110–9115 (2018).
46. Slootman, J., Yeh, C. J., Millereau, P., Comtet, J. & Creton, C. A molecular interpretation of the toughness of multiple network elastomers at high temperature. *Proc. Natl Acad. Sci. USA* **119**, e2116127119 (2022).
47. Chen, Y., Yeh, C. J., Qi, Y., Long, R. & Creton, C. From force-responsive molecules to quantifying and mapping stresses in soft materials. *Sci. Adv.* **6**, eaaz5093 (2020).
48. Liu, Z., Zakoworotny, M., Guo, J., Zehnder, A. T. & Hui, C.-Y. Energy release rate of a single edge cracked specimen subjected to large deformation. *Int. J. Fract.* **226**, 71–79 (2020).
49. Greensmith, H. W. Rupture of rubber. X. The change in stored energy on making a small cut in a test piece held in simple extension. *J. Appl. Polym. Sci.* **7**, 993–1002 (2003).
50. Rogers, J. A. Materials and mechanicsfor stretchable electronics. *Sicence* **237**, 1603–1606 (2010).
51. Schauser, N. S. et al. The role of backbone polarity on aggregation and conduction of ions in polymer electrolytes. *J. Am. Chem. Soc.* **142**, 7055–7065 (2020).
52. Angel, C. A. Mobile ions in amorphous solids. *Annu. Rev. Phys. Chem.* **43**, 693–717 (1992).
53. Diederichsen, K. M., Buss, H. G. & McCloskey, B. D. The compensation effect in the Vogel–Tammann–Fulcher (VTF) Equation for Polymer-Based Electrolytes. *Macromolecules* **50**, 3831–3840 (2017).
54. Chen, L. et al. Facile synthesis of novel elastomers with tunable dynamics for toughness, self-healing and adhesion. *J. Mater. Chem. A* **7**, 17334–17344 (2019).
55. Sun, J., Stone, G. M., Balsara, N. P. & Zuckermann, R. N. Structure–conductivity relationship for peptoid-based PEO–mimetic polymer electrolytes. *Macromolecules* **45**, 5151–5156 (2012).

56. He, R. & Kyu, T. Effect of plasticization on ionic conductivity enhancement in relation to glass transition temperature of cross-linked polymer electrolyte membranes. *Macromolecules* **49**, 5637–5648 (2016).
57. Wang, Y. et al. Decoupling of ionic transport from segmental relaxation in polymer electrolytes. *Phys. Rev. Lett.* **108**, 088303 (2012).
58. Williams, M. L., Landel, R. F. & Ferry, J. D. The temperature dependence of relaxation mechanisms in amorphous polymers and other glass-forming liquids. *J. Am. Chem. Soc.* **77**, 3701–3707 (1955).
59. Zhang, W. et al. Fatigue of double-network hydrogels. *Eng. Fract. Mech.* **187**, 74–93 (2018).
60. Tanaka, M. & Mochizuki, A. Clarification of the blood compatibility mechanism by controlling the water structure at the blood-poly(-meth)acrylate interface. *J. Biomater. Sci. Polym. Ed.* **21**, 1849–1863 (2010).

Acknowledgements

B.Y. gratefully acknowledges funding from the Chinese Scholarship Council (File NO: 202106320186) for her stay at the ESPCI Paris and the Excellence of Science (EOS 40007519) program from the FWO and FRS-FNRS for financial support. We thank also Dr. Victoria Waltz and Dr. Atul Sharma for their help with the synthesis of the samples.

Author contributions

B.Y. and C.C. conceived the idea and designed the research. B.Y. synthesized the samples and performed the mechanical characterizations. B.Y., S.H., A.C., and G.M. conducted the EIS, chemical, and thermal experiments. B.B., A.R., and C.C. analyzed and interpreted the results. All authors discussed the data. B.Y. and C.C. wrote the paper with contributions from all authors.

Competing interests

The authors declare no competing interests.

Additional information

Supplementary information The online version contains supplementary material available at https://doi.org/10.1038/s41467-024-55472-8.

Correspondence and requests for materials should be addressed to Costantino Creton.

Peer review information *Nature Communications* thanks the anonymous reviewers for their contribution to the peer review of this work. A peer review file is available.